

This article was downloaded by:

On: 15 January 2011

Access details: *Access Details: Free Access*

Publisher *Taylor & Francis*

Informa Ltd Registered in England and Wales Registered Number: 1072954 Registered office: Mortimer House, 37-41 Mortimer Street, London W1T 3JH, UK



Journal of Experimental Nanoscience

Publication details, including instructions for authors and subscription information:

<http://www.informaworld.com/smpp/title~content=t716100757>

pH-Dependent gold nanoparticle self-organization on functionalized Si/SiO₂ surfaces

S. Diegoli^a; P. M. Mendes^a; E. R. Baguley^a; S. J. Leigh^a; P. Iqbal^a; Y. R. Garcia Diaz^a; S. Begum^a; K. Critchley^b; G. D. Hammond^c; S. D. Evans^b; D. Attwood^d; I. P. Jones^c; J. A. Preece^a

^a School of Chemistry, The University of Birmingham, UK ^b Department of Physics and Astronomy, The University of Leeds, UK ^c School of Physics and Astronomy, The University of Birmingham, UK ^d Materials Sciences Department, BAE SYSTEMS, UK ^e School of Metallurgy and Materials, The University of Birmingham, UK

To cite this Article Diegoli, S. , Mendes, P. M. , Baguley, E. R. , Leigh, S. J. , Iqbal, P. , Diaz, Y. R. Garcia , Begum, S. , Critchley, K. , Hammond, G. D. , Evans, S. D. , Attwood, D. , Jones, I. P. and Preece, J. A. (2006) 'pH-Dependent gold nanoparticle self-organization on functionalized Si/SiO₂ surfaces', *Journal of Experimental Nanoscience*, 1: 3, 333 – 353

To link to this Article: DOI: 10.1080/17458080600778644

URL: <http://dx.doi.org/10.1080/17458080600778644>

PLEASE SCROLL DOWN FOR ARTICLE

Full terms and conditions of use: <http://www.informaworld.com/terms-and-conditions-of-access.pdf>

This article may be used for research, teaching and private study purposes. Any substantial or systematic reproduction, re-distribution, re-selling, loan or sub-licensing, systematic supply or distribution in any form to anyone is expressly forbidden.

The publisher does not give any warranty express or implied or make any representation that the contents will be complete or accurate or up to date. The accuracy of any instructions, formulae and drug doses should be independently verified with primary sources. The publisher shall not be liable for any loss, actions, claims, proceedings, demand or costs or damages whatsoever or howsoever caused arising directly or indirectly in connection with or arising out of the use of this material.

pH-Dependent gold nanoparticle self-organization on functionalized Si/SiO₂ surfaces

S. DIEGOLI[†], P. M. MENDES[†], E. R. BAGULEY[†], S. J. LEIGH[†], P. IQBAL[†],
Y. R. GARCIA DIAZ[†], S. BEGUM[†], K. CRITCHLEY[‡], G. D. HAMMOND[§],
S. D. EVANS[‡], D. ATTWOOD[¶], I. P. JONES^{||} and J. A. PREECE^{*†}

[†]School of Chemistry, The University of Birmingham, UK

[‡]Department of Physics and Astronomy, The University of Leeds, UK

[§]School of Physics and Astronomy, The University of Birmingham, UK

[¶]Materials Sciences Department, BAE SYSTEMS, UK

^{||}School of Metallurgy and Materials, The University of Birmingham, UK

(Received December 2005; in final form June 2006)

The self-organization of citrate- and acrylate-stabilized gold nanoparticles onto SiO₂/hydroxyl-, amino- and nitro-terminated surfaces was investigated as a function of pH. Bare clean Si/SiO₂ substrates were used as the SiO₂/hydroxyl-terminated surfaces and self-assembled monolayers (SAM) of (3-aminopropyl)trimethoxysilane (APTMS) and 3-(4-nitrophenoxy)-propyltrimethoxysilane (NPPTMS) on Si/SiO₂ were employed as the amino- and nitro-terminated surfaces, respectively. All the surfaces were fully characterized by contact angle, atomic force microscopy (AFM), ellipsometry and X-ray photoelectron spectroscopy (XPS). Citrate- and acrylate-stabilized gold nanoparticle stability was also investigated as a function of pH by UV–visible absorption spectroscopy and Z-potentiometry. The gold nanoparticle surface coverage of the substrates was independently estimated by AFM and XPS. The results show that colloid deposition on bare SiO₂/OH surfaces and on NPPTMS monolayers is negligible with the exception of acrylate-stabilized gold nanoparticles which were found to be immobilized on nitro-terminated surfaces at pH lower than 3.5. Nevertheless, APTMS monolayers interact strongly with citrate- and acrylate-stabilized gold nanoparticles exhibiting a dependence of the surface coverage from the pH of the colloidal solution.

Keywords: AFM; Gold nanoparticles; Nanostructures; Self-organization; XPS

1. Introduction

The immobilization of metal nanoparticles on different substrates to form three-dimensional nano-architectures has been the subject of interdisciplinary research due to the potential applications in the areas of electronics, photonics, sensors and catalysis [1–4]. However, the key step to realizing these applications is to gain precise spatial

*Corresponding author. Email: J.A.Preece@bham.ac.uk

control over nanoparticle assembly on suitable surfaces [1, 5]. To this end, a possibility is provided from hybrid top-down/bottom-up approaches. In this scenario top-down, high-resolution, lithographic techniques are used to nanostructure surfaces of technologically relevant materials and self-assembly techniques from the bottom-up approach are employed to organize nano-entities on the patterns [6].

Self-assembled monolayers (SAMs) are ideal resists for patterning high-resolution features because they provide a well-defined organic substrate that can be modified by exposure to various types of radiations [6]. Moreover, SAMs can be tailored by a suitable choice of their molecular building blocks to provide possibilities for non-conventional lithographic approaches such as chemical lithography. Along this research line detailed investigations have been already carried out on the chemical patterning of surfaces with X-rays [7] and high-energy electrons [8] including chemical modification of nitro-terminated SAMs on Si/SiO₂ substrates to amino-terminated SAMs. Furthermore, the nitro-/amino-patterned monolayers have been employed as templates to guide the self-organization of negatively charged citrate-stabilized gold nanoparticles via electrostatic interactions with the protonated amino sites [8]. However, a fundamental study of the deposition of colloidal particles from solution onto different substrates of well-defined surface chemistry under a range of conditions would allow better control over specificity and selectivity of the self-organization process on chemically patterned surfaces.

In this paper, a systematic investigation on the immobilization of citrate- and acrylate-stabilized gold nanoparticles onto SiO₂/hydroxyl-, amino- and nitro-terminated surfaces as a function of pH is reported.

Previous work has addressed the study of the attachment of gold nanoparticles on different SAMs [8, 9–12]. However, to our knowledge, systematic studies concerning pH-dependent immobilization of both citrate- and acrylate-stabilized gold nanoparticles under the same conditions have not been reported.

2. Experimental section

2.1. Materials

Commercially available chemicals and solvents were purchased from Aldrich and Fisher Scientific and were used as received. Anhydrous THF was dried over Na/benzophenone and distilled under a N₂ atmosphere. Prime grade and p-doped (dopant B) silicon (Si/SiO₂) wafers were purchased from Virginia Semiconductor, Inc. These wafers came polished on one side with (111) orientation, a resistivity of 11–21 Ω cm and a thermally grown 100 nm thick oxide layer on both sides.

2.2. Gold nanoparticles

2.2.1. Citrate-stabilized gold nanoparticles. The nanoparticle solution was synthesized by the Frens method [13]. An aqueous solution (100 ml) of H₂AuCl₄ · 3H₂O (9.9 mg, 2.5 × 10⁻² mmol) was heated under reflux for 5–10 minutes, and an aqueous solution (2 ml) of sodium citrate (22.8 mg, 7.8 × 10⁻² mmol) was added. Heating was continued

for a further 10 minutes to ensure complete reduction of the gold salt. The colloidal gold solution was centrifuged for 10 minutes at 3500 rpm and the supernatant collected.

2.2.2. Acrylate-stabilized gold nanoparticles. The nanoparticle solution was prepared as described previously [14]. An aqueous solution (50 ml) of HAuCl₄ · 3H₂O (19.7 mg, 5.0×10^{-2} mmol) was heated under reflux for 5–10 minutes, and a warm (50–60°C) aqueous solution (15 ml) of sodium acrylate (112.86 mg, 2.5×10^{-2} mmol) was added quickly. Heating was continued for further 30 minutes until a deep-red solution was observed. The particle solution was centrifuged for 10 minutes at 3500 rpm and the supernatant collected.

2.2.3. UV–visible absorption spectroscopy. Gold nanoparticle solutions were characterized by UV–visible absorption spectroscopy, using a Hewlett-Packard 8452A spectrometer.

2.2.4. Transmission electron microscopy (TEM). Micrographs of citrate- and acrylate-stabilized gold nanoparticles were collected on a JEOL 1200EX transmission electron microscope operating at 120 kV. Samples were prepared by slow evaporation of one drop of the as-prepared nanoparticle solution on a carbon coated copper grid.

2.2.5. Zeta potentiometry. Zeta potential measurements were performed using a Malvern Instruments Zetasizer 1000Hs, operating with a variable power (5–50 mW) He–Ne laser at 633 nm. Measurements were taken at 25°C, and repeated eight times. Before, and in between measurements, the flow through cell was washed with ultra-high pure (UHP) water (10 ml).

2.2.6. pH Measurements. pH Analysis were performed with a IQ150 pH meter from IQ Scientific Instruments, Inc. The pH of the gold nanoparticle solutions was changed without significantly altering the concentration of the colloidal solution. A very small amount ($\leq 50 \mu\text{l}$) of an NaOH or HCl aqueous solution of optimum concentration was added to the colloidal solution (4 ml) to achieve the desired pH value.

2.3. Synthesis of 3-(4-nitrophenoxy)-propyltrimethoxysilane (NPPTMS)

2.3.1. 1-Allyloxy-4-nitro-benzene. A solution of 4-nitrophenol (20 g, 0.14 mol), allyl chloride (13.21 g, 0.17 mol), K₂CO₃ (39.71 g, 0.29 mol) and NaI (10.88 g, 0.07 mol) in acetone (150 ml) was stirred for 20 hours at room temperature. The reaction mixture was filtered and the filtrate was concentrated *in vacuo*. The crude product was purified by silica gel column chromatography (graded elution: 0% to 15% EtOAc in hexane, increments of 5% per 150 ml of eluent used). The solvent was removed *in vacuo* to yield a yellow solid (21.91 g, 85%). ¹H NMR (300 MHz, CDCl₃): mp: 35–36°C; δ_{H} 8.20 (d, $J = 9.38$ Hz, 2H, Ar–H), 6.96 (d, 9.38 Hz, 2H, Ar–H), 6.10–5.97 (m, 1H, CH=CH₂), 5.43 (dd, $J = 17.28, 1.35$ Hz, 1H, CH₂=CH), 5.35 (dd, $J = 10.67, 1.35$ Hz, CH₂=CH), 4.64 (d, $J = 5.52$ Hz, 2H, OCH₂); ¹³C NMR (75 MHz, CD₃Cl): δ_{C} 163.1, 141.5, 130.8,

124.8, 117.6, 113.7, 68.4; ν/cm^{-1} (nujol): 3086, 2928, 2898, 1610, 1594, 1521, 1497; m/z (EIMS): 179 ($[\text{M}]^+$, 100%).

2.3.2. 3-(4-Nitrophenoxy)-propyltrimethoxysilane. To a solution of 1-allyloxy-4-nitrobenzene (10 g, 0.06 mol) in trimethoxysilane (13.65 g, 0.11 mol) under N_2 atmosphere, a solution of H_2PtCl_6 in dry $^i\text{PrOH}$ (0.3 ml, 0.04 M) was added. The reaction mixture was stirred under N_2 atmosphere for 20 hours at 40°C . The mixture was cooled to room temperature and the excess trimethoxysilane removed *in vacuo* to yield a pale yellow solid. The solid was recrystallized in a solution of hexane and EtOH (20:1) (14.01 g, 83%). mp: $44\text{--}46^\circ\text{C}$; ^1H NMR (300 MHz, CDCl_3): δ_{H} 8.18 (d, $J=9.20$ Hz, 2H, Ar-H), 6.93 (d, 9.20 Hz, 2H, Ar-H), 4.02 (t, $J=6.44$ Hz, 2H, OCH_2), 3.58 (s, 9H, OMe), 1.97–1.88 (m, 2H, CH_2), 0.79 (m, 2H, CH_2Si); ^{13}C NMR (75 MHz, CDCl_3): δ_{C} , 163.2, 140.1, 125.0, 113.6, 69.6, 49.7, 21.5, 3.5; ν/cm^{-1} (nujol): 2922, 2898, 1593, 1514, 1499; m/z (ESMS): 324 ($[\text{M} + \text{Na}]^+$, 100%). The HPLC analysis indicated that the product was 67% pure and MS indicated that it did not contain any other trimethoxysilane derivative. Attempts to further purify the NPPTMS were not successful. Similar purification difficulties have been previously reported [15–16].

2.3.3. NMR spectroscopy. ^1H NMR spectra were recorded on a Bruker AC 300 (300 MHz) and ^{13}C NMR spectra were recorded on a Bruker AV 300 (75.5 MHz). All chemical shifts are quoted in ppm to higher frequency from Me_4Si using either deuterated chloroform (CDCl_3) as the lock and the residual solvent as the internal standard. The coupling constants are expressed in Hertz (Hz) with multiplicities abbreviated as follows: s=singlet, d=doublet, dd=double doublet, t=triplet, q=quartet and m=multiplet.

2.3.4. Mass spectroscopy (MS). Electrospray Mass Spectrometry (ESMS) was performed on a Micromass Time of Flight (TOF) using methanol as the running solvent. Electron impact (EI) mass spectra were recorded at 70 eV on a VG ProSpec mass spectrometer.

2.3.5. Infrared spectroscopy (IR). IR spectra were recorded as thin solid films on NaCl disks using a Perkin Elmer Paragon 1000 FT-IR.

2.3.6. Thin-layer chromatography (TLC). TLC analysis were carried out on aluminium plates coated with silica gel 60 F254 (Merck 5554). The TLC plates were air-dried and analysed under a short-wave UV lamp (254 nm). Column chromatographic separations were performed on silica gel 120 (ICN Chrom 32–63, 60 Å).

2.3.7. High-performance liquid chromatography (HPLC). HPLC analysis were recorded on a Dionex Summit HPLC System with Chromeleon Software, using a Summit UVD 170s UV/VIS Multi-Channel Detector with analytical flow cell. Analytical RP-HPLC runs were performed on a Luna (Phenomenex), C_{18} , 250 mm \times 4.6 mm ID,

with 10 μm pore size column using a gradient of MeCN/H₂O [(60/40) + 0.05% TFA], from 0–100% over 80 minutes.

2.4. Self-assembled monolayers

2.4.1. Self-assembled monolayer preparation. Prior to cleaning of Si/SiO₂ wafers and preparation of SAMs, all glassware was thoroughly cleaned. Contaminants were removed with piranha solution (conc. H₂SO₄: 30% H₂O₂ = 7:3) followed by rinsing with UHP H₂O (Resistivity = 18 MΩcm) (*caution: piranha solution reacts violently with organic materials and should be handled carefully*). The subsequent cleaning steps were as follows: 30 minutes sonication in UHP water; rinsing with EtOH; 30 minutes sonication in EtOH; and finally rinsing thoroughly with EtOH. The glassware was then dried in an oven (≈120°C) for a minimum of 24 hrs.

The silicon wafers were cut into approximately 1 cm² pieces, and cleaned according to the following protocol [15, 17–18]. The silicon wafers were immersed in piranha solution at 90–100°C for 60 minutes. Once cooled, the substrates were rinsed with UHP H₂O, and then sonicated in RCA solution (UHP H₂O:30% H₂O₂:NH₄OH = 5:1:1) for 1 hour at room temperature. Finally, the substrates were rinsed repeatedly with UHP H₂O and stored in UHP H₂O. The clean silicon wafers were used within two days due to the loss of surface hydrophilicity for longer storage times.

For (3-aminopropyl)trimethoxysilane (APTMS) monolayers preparation, the cleaned silicon substrates were transferred from UHP H₂O into EtOH by stepwise exchange of the solvents (H₂O:EtOH ratio of 3:1; 2:2; 1:3; EtOH; anhydrous EtOH). The wafers were immersed, under Ar atmosphere, into a 0.5 mM solution of APTMS in anhydrous EtOH (5 ml) and sonicated at 25°C for 1 hour. The formation of SAMs was carried out under ultrasonication to prevent physisorption of any polymeric siloxanes. Upon removal from the solution, the substrates were rinsed thoroughly with EtOH and CHCl₃, sonicated twice in fresh EtOH and rinsed once more with EtOH and CHCl₃ in order to remove physisorbed material from the surface. Each sample was dried with a stream of Ar and cured at 120°C for 30 minutes under vacuum. The same procedure was used for the formation of 3-(4-nitrophenoxy)-propyltrimethoxysilane (NPPTMS) monolayers, but sonication was carried out for 2 hours at a concentration of 2.5 mM and THF, rather than EtOH, was used as the solvent.

2.4.2. Immersion of bare and functionalized Si/SiO₂ substrates in gold nanoparticle solutions. The citrate-stabilized gold nanoparticle solution was used as-prepared. The acrylate-stabilized gold nanoparticle solution was diluted by adding three parts of water for each part of acrylate-stabilized gold nanoparticle solution to afford a concentration comparable with the one of the citrate-stabilized gold nanoparticle solution. Samples were immersed in 4 ml of citrate- and acrylate-stabilized gold nanoparticle solutions at pH 3.0, 3.5, 4.0, 4.5, 5.0 and 5.5 for 2 hours. After immersion, the substrate was rinsed with UHP water for 1 minute and dried under a stream of Ar.

2.4.3. Contact angle. Water contact angles were determined by the sessile drop method using a home built contact angle apparatus, equipped with a CCD camera that

is attached to a personal computer for video capture. The advancing (θ_a) and receding (θ_r) contact angles were measured as a micro-syringe was used to quasi-statically add liquid to or remove liquid from the drop. The drop is shown as a live video image on the PC screen and digitally recorded for future analysis. The acquisition rate was four frames per second. Stored images of droplets were analysed by using software from FTA. Contact angles were determined from an average of five different measurements on each sample.

2.4.4. Ellipsometry. The thickness of the deposited monolayers was determined by multiwavelength spectroscopic ellipsometry. A Jobin-Yvon UVISSEL ellipsometer with white light source was used for the measurements. The angle of incidence was fixed at 70° and the compensator was set at -45° . A wavelength range of 220–820 nm was used. The ellipsometric parameters, Δ and ψ , were determined for both the bare clean substrate and the SAM. The DeltaPsi software was employed to determine the thickness values using a Cauchy oscillator model. The thickness reported is the average of six measurements taken on the same sample.

2.4.5. X-Ray photoelectron spectroscopy (XPS). XPS spectra were obtained on a VG ESCALAB 250 controlled by an Avantage data system. XPS experiments were carried out using a monochromatic Al K_α X-ray source (1486.6 eV) operated at 15 kV and 150 W. The pressure in the spectrometer was in the range 10^{-8} – 10^{-9} torr. Si (2p), C (1s), O (1s), N (1s), Au (4f) spectra were recorded using a pass energy of 20 eV and a step size of 0.10 eV. Fitting of XPS peaks was performed using the spectra processing program in the XPS software. The Au/Si ratios of the nanoparticle films were determined from the peak areas of the elements.

2.4.6. Atomic force microscopy (AFM). The surface topography of the films before and after immersion in gold nanoparticle solutions was imaged using a multimode Nanoscope IIIA system (Digital Instruments, Santa Barbara, CA) operated in tapping mode using etched silicon probes with a nominal spring constant of 20–80 N/m and a tip radius <10 nm (model RTESP, Veeco Instruments, Inc). AFM images were acquired in air as 512×512 pixels with a scan rate of 1.00 Hz. Surface roughness (R_{rms}) and coverage were determined with a scan range image of $500 \text{ nm} \times 500 \text{ nm}$. At least four different areas were analysed to obtain statistical data for surface roughness and coverage. Although AFM images of $500 \text{ nm} \times 500 \text{ nm}$ were used to investigate the surface coverage, lower resolution images of $3 \mu\text{m} \times 3 \mu\text{m}$ were also taken to assess the large scale coverage of the substrate. The convoluted surface coverage of the nanoparticles in the AFM images was determined using the flooding function of the WSxM software. The true surface coverage area (Area_T) was accessed using the product of the convoluted surface coverage area (Area_C) by the ratio of the true particle diameter squared (d_T) to the convoluted particle diameter squared (d_C): $\text{Area}_T = \text{Area}_C \times (d_T^2/d_C^2)$. The Nanoscope software applied to $500 \text{ nm} \times 500 \text{ nm}$ AFM images was used for the determination of the convoluted particle diameter. The AFM height of the particles deposited on the substrates was assessed through cross-section analysis of the AFM images using Nanoscope software.

3. Results and discussion

3.1. Gold nanoparticle stability as a function of pH

A prerequisite for studying how citrate- and acrylate-stabilized gold nanoparticles self-organize on substrates of defined surface chemistry from solution is to ensure that the colloids are stable under the range of experimental conditions explored. Citrate- and acrylate-stabilized gold nanoparticles were prepared as described in the experimental section and were characterized by TEM and UV–visible absorption spectroscopy before altering the pH of the colloidal solutions. TEM micrographs of the gold nanoparticles are shown in figure 1, and their physical data are summarized in table 1. UV–visible absorption spectroscopy was also used to monitor the stability of the colloidal solutions as a function of pH (figure 2). It is well-known that the position and shape of the plasmon resonance band are strongly related with particle size, dispersity and degree of aggregation [19–23]. In particular, the maximum of the surface plasmon band moves to longer wavelength with increasing particle size and an increase in peak width at half maximum is related to increasing particle dispersity. For citrate- and acrylate-stabilized gold nanoparticles the maximum of the surface plasmon band was observed at 520 nm and 530 nm, respectively, as reported in table 1. The difference in the plasmon resonance band for the two colloidal solutions can be rationalized by taking into account the difference of about 20% in nanoparticle diameter measured by TEM. As a consequence, the surface plasmon band of acrylate-stabilized gold nanoparticle solutions is red shifted consistently with the larger particle size. It can also be observed in figure 2, that the surface plasmon band of the acrylate-stabilized gold nanoparticles

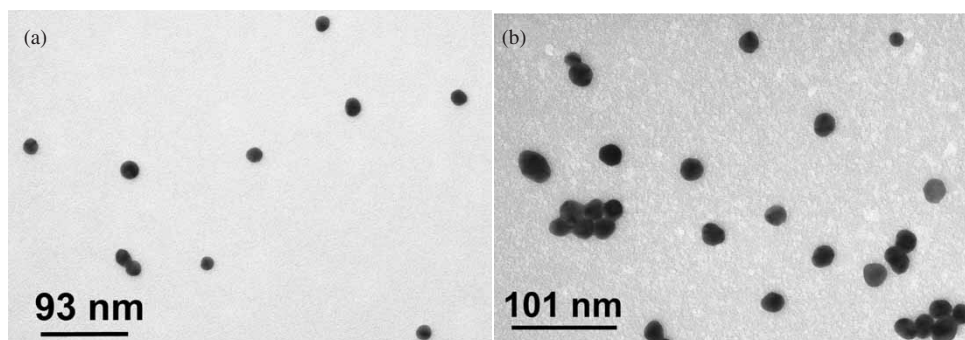


Figure 1. TEM of (a) citrate- and (b) acrylate-stabilized gold nanoparticles.

Table 1. Characterization of citrate- and acrylate-stabilized Au nanoparticles.

Stabilizer	Plasmon resonance (nm)	Nanoparticle size (nm)		
		TEM	AFM height	AFM width
Citrate	520	15.8 ± 1.9	18.4 ± 4.3	31.1 ± 6.0
Acrylate	530	19.7 ± 3.3	19.0 ± 3.8	39.9 ± 6.3

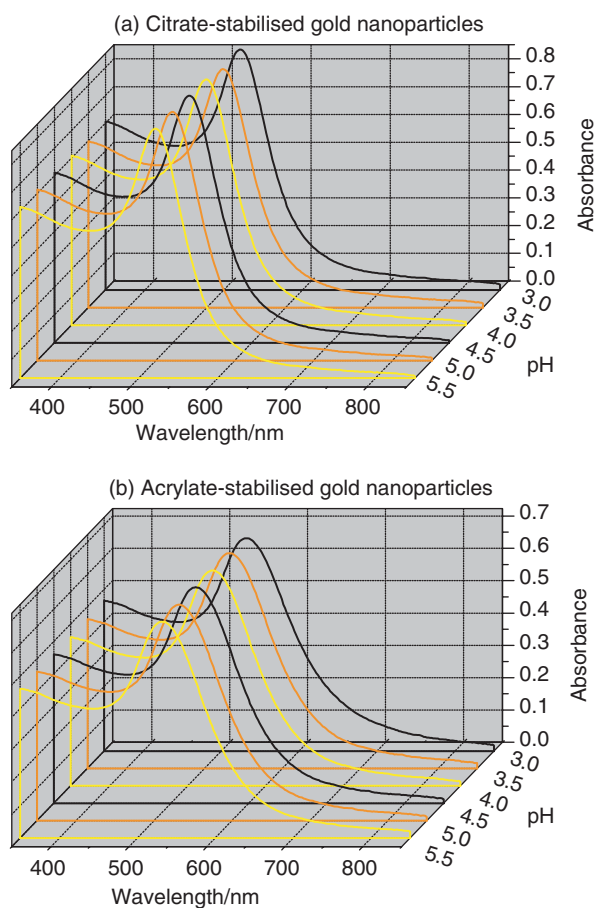


Figure 2. UV-visible absorption spectroscopy of (a) citrate- and (b) acrylate-stabilized gold nanoparticle solutions as a function of pH. The UV-visible spectra were collected 24 hours after changing the pH of the solutions and were nearly identical to the spectra recorded at its original pH.

solutions is broader compared with the one of citrate-stabilized gold nanoparticle solutions. This result is in agreement with the higher dispersity of the acrylate-stabilized gold nanoparticle size distributions obtained by TEM. Furthermore, the position and shape of the surface plasmon band did not exhibit any dependence from the pH of the colloidal solution indicating good stability of citrate- and acrylate-stabilized gold nanoparticle solutions over the range of conditions explored (figure 2).

The surface charge of the gold nanoparticles was examined as a function of pH by zeta potentiometry as reported in figure 3. The zeta potential of a colloidal solution is an indicator of its stability [24]. The greater the zeta potential, the higher is the repulsion between the particles. As an empirical rule [24], colloidal suspensions exhibiting zeta potentials lying in the interval between -30 mV and $+30$ mV are generally unstable. Therefore, colloidal suspensions are considered stable when their zeta potentials are more positive than $+30$ mV or more negative than -30 mV.

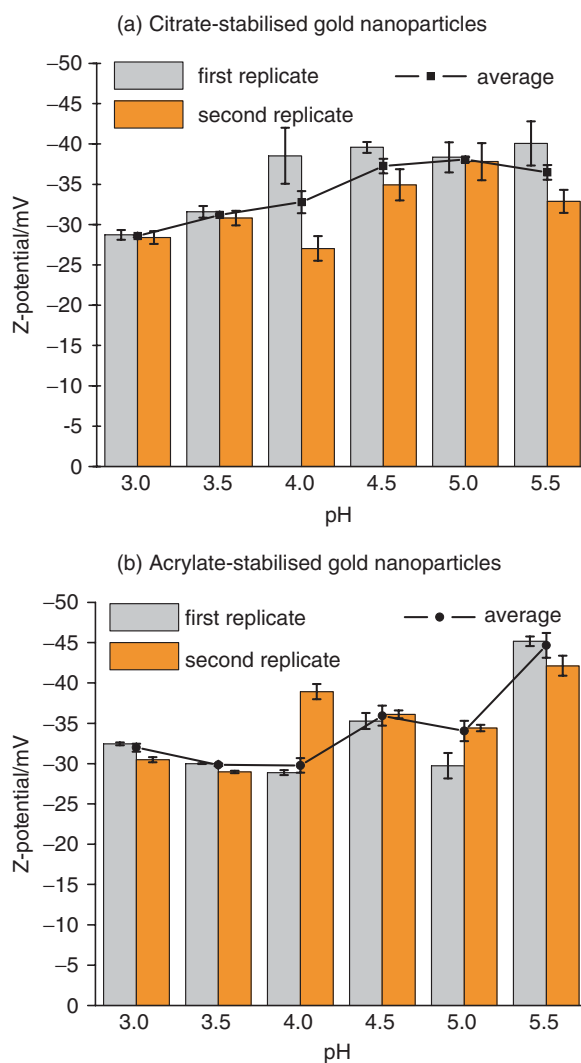


Figure 3. Zeta potential of (a) citrate- and (b) acrylate-stabilized gold nanoparticles measured between pH 3.0 and pH 5.5. The zeta potential was measured 10 minutes after changing the pH.

Citrate- and acrylate-stabilized gold nanoparticles are negatively charged and the zeta potential measurements indicate good stability of both the colloidal solutions over the range of pHs explored. It can also be observed that the zeta potential of both the colloidal solutions becomes less negative in acidic pHs as shown in figure 3. Although the exact chemical nature of the passivant adsorbed on the surface of citrate- and acrylate-stabilized gold nanoparticles is not definitively known [25], an attempt can be made to rationalize the observed trend. There is some evidence showing that citrate ions, chloride, gold chloride (AuCl_4^- and AuCl_2^- produced by incomplete reduction of AuCl_4^-) and hydroxide anions are present on the citrate-stabilized gold nanoparticle

surface [12, 23, 25–26]. When the pH becomes more acidic a progressive protonation of all these species occurs. As a consequence the surface of the gold colloids becomes less negatively charged in agreement with the trend in figure 3.

In conclusion, the UV–visible spectra and the zeta potential measurements suggest that both citrate- and acrylate-stabilized gold nanoparticles are stable in solution in the pH range used in the experiments presented here and the surface charge of the colloids becomes less negative when the solution becomes more acidic.

3.2. Characterization of the Si/SiO₂ surface and the SAMs of NPPTMS and APTMS

For the purposes of this study, the full characterization of the substrates used is of paramount importance as it has been proved that the quality of the surfaces is crucial for the accurate assessment of the nanoparticles coverage [27]. Si/SiO₂ substrates were cleaned as described in the experimental section and used as the SiO₂/hydroxyl-terminated surfaces. SAMs of (3-aminopropyl)trimethoxysilane (APTMS) and 3-(4-nitrophenoxy)-propyltrimethoxysilane (NPPTMS) were formed as reported in the experimental section and they have been used as the amino- and nitro-terminated surfaces, respectively. Silane-based monolayers are experimentally difficult to self-assemble. This difficulty arises from their formation mechanism which requires high control over the water content of the adsorbate solution for the formation of good quality SAMs. It has been demonstrated that a water film (one or several molecular layers thick) covering the substrate is necessary for the formation of a complete monolayer [28, 29]. On the other hand, a too high content of water in the organosilane solution promotes the formation of oligomeric siloxanes that results in the deposition of a multilayered structure and an increase in the film roughness [30]. Therefore, APTMS and NPPTMS SAMs were characterized by contact angle, ellipsometry, and AFM (these data are summarized in table 2), as well as XPS. The clean bare Si/SiO₂ substrates displayed low advancing and receding water contact angles (θ_a and $\theta_r < 10^\circ$) indicative of highly hydroxylated and clean surfaces prior to modification. After APTMS SAM formation, the advancing and receding contact angles increased to 57° and 30° , respectively. Comparable data were obtained with NPPTMS SAMs, i.e. 61° and 30° for advancing and receding contact angles, respectively (table 2). The contact angle values achieved are in good agreement with literature [8, 31]. The monolayer thickness determined by ellipsometry for APTMS and NPPTMS were (0.5 ± 0.1) nm

Table 2. Characterization of the surfaces studied.

Surface	Contact angle ($^\circ$)		Thickness (nm)		Roughness ^c (nm)
	Advancing	Receding	Theoretical ^a	Experimental ^b	
Si/SiO ₂	<10	<10	–	–	0.40 ± 0.03
APTMS	57 ± 4	30 ± 3	0.5	0.5 ± 0.1	0.33 ± 0.03
NPPTMS	61 ± 5	30 ± 3	1.1	0.9 ± 0.2	0.34 ± 0.03

^aDetermined using the SPARTAN molecular modelling software.

^bDetermined by ellipsometry.

^cDetermined by AFM.

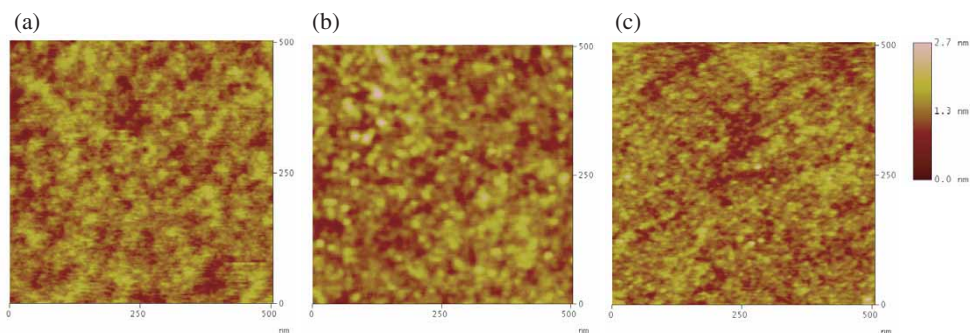


Figure 4. Tapping mode AFM images (500 nm \times 500 nm) of (a) clean Si/SiO₂, (b) NPPTMS monolayer on Si/SiO₂ and (c) APTMS monolayer on Si/SiO₂.

and (0.9 ± 0.2) nm, which were in good agreement with the calculated molecular lengths as reported in table 2.

AFM topography measurements were used to gain further information on the morphology of bare Si/SiO₂ substrates and amino- and nitro-terminated SAMs (figure 4). AFM images showed that NPPTMS and APTMS monolayers are homogeneous, smooth and do not feature any noticeable aggregation. It is noteworthy that the roughness values obtained for APTMS and NPPTMS monolayers were smaller than the roughness values obtained for clean Si/SiO₂ substrates (table 2). This smoothing effect has been ascribed to the cross-linkage of the silane chains, such that the complete monolayer can be pictured as a carpet where all the chains are interconnected with each other, but just a few are actually adsorbed onto the Si/SiO₂ surface holding the film on the substrate [32]. Therefore, the resulting monolayer smoothes the substrate surface. Similar results for surface roughness and homogeneity of these substrates were obtained when larger areas were scanned.

The chemical structure and composition of bare and modified Si/SiO₂ surfaces was characterized by XPS. XPS Confirmed SAM formation, showing signals from Si (2p), C (1s), O (1s) and N (1s). High-resolution scans of the Si (2p) region show the presence of only a band at 102.5 eV associated with silicon bound to oxygen. The absence of the Si (2p) signal from the bulk substrate at 100 eV, characteristic of silicon-silicon bonds, was attributed to the strong attenuation from the 100-nm-thick thermally grown silicon oxide used in these studies. The N (1s) peak of the APTMS monolayer showed two broad overlapping signals, one at a binding energy of 400.1 eV, and a second at 402.1 eV, which are characteristic of an amine and a protonated amine group, respectively (figure 5a) [7]. XPS Measurements also confirmed the adsorption of NPPTMS on Si/SiO₂ by the observation of both the NO₂ and NH₂ N(1s) binding energies (figure 5b). As it has been previously observed [7, 8], the NO₂ groups (N(1s) binding energy = 405.7 eV) in SAMs of NPPTMS are gradually reduced to NH₂ groups during X-ray irradiation initiated by the photoelectrons and secondary electrons emitted from the surface [33]. It is worth noting that the NH₂ peak obtained from the X-ray chemical conversion can also be deconvoluted into an amine (400.0 eV) and a protonated amine (401.8 eV). From the SAM analysis, it can then be concluded

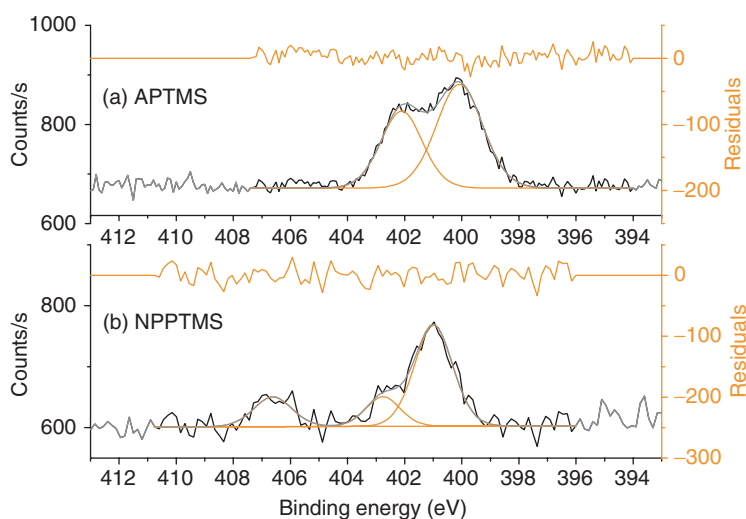


Figure 5. XPS N(1s) spectra of a monolayer of (a) APTMS and (b) NPPTMS on Si/SiO₂ taken after 15 minutes of continuous exposure to X-ray irradiation.

that APTMS and NPPTMS form uniform, smooth, densely packed molecular layers on Si/SiO₂.

3.3. Gold nanoparticle deposition

Colloid deposition from solution onto a solid surface is a complex process, where many variables such as concentration, pH and ionic strength of the colloidal solution, immersion time, particle size and substrate surface chemistry are expected to play a major role [9, 10, 12]. In this study, the attention was focused on the effect of pH, stabilizing agent, and substrate surface chemistry, therefore the concentration of the colloidal solutions and the immersion time were kept constant throughout the experiments as reported in the experimental section. The addition of acid and base to the gold nanoparticles will change the ionic strength of the solution. Therefore, we attempted to suspend the particles in aqueous 0.1 M NaCl solution because at this salt concentration the ionic strength would vary by less than 10% upon pH variation. However, the particles were not stable under these conditions and precipitation occurred. It should be also noted that citrate-stabilized gold nanoparticles have a diameter $\sim 20\%$ smaller than the acrylate particles. Thus, acrylate-stabilized gold nanoparticles would expect to have a greater propensity to self-organize more readily to surfaces than the citrate-stabilized gold nanoparticles, based on contact areas. This premise was found to be contradicted by the experimental evidence, and thus the dominating factor for the self-organization is the surface chemistry of the gold nanoparticles interacting with the planar surfaces, and not the surface contact area.

The coverage of the gold nanoparticles on the functionalized surfaces was independently evaluated using AFM and XPS. At least four different AFM images $500\text{ nm} \times 500\text{ nm}$ ($2.5 \times 10^5\text{ nm}^2$) were used for the determination of the surface

coverage for each substrate. Lower resolution 3.0 $\mu\text{m} \times 3.0 \mu\text{m}$ AFM images were also collected to assess the homogeneity of the gold nanoparticle coverage. The lateral dimensions of the nanoparticles in the AFM images were considerably larger than the values determined from TEM measurements (table 1). This deviation is attributed to the convolution effect of the nanoparticles with the AFM tip [34, 35] and has to be taken into account when determining the surface coverage area from AFM images as described in the experimental section. Nevertheless, if a section analysis is performed on the AFM image, the nanoparticle height is in good agreement with the nanoparticle size determined by TEM (table 1). Representative 500 nm \times 500 nm AFM images of Si/SiO₂ substrates, NPPTMS and APTMS monolayers after immersion in the citrate- and acrylate-stabilized gold nanoparticle solutions at different pHs are shown in figures 6, 7 and 8, respectively. The XPS surface coverage has been calculated as the ratio of the integrated areas of the Au 4f peaks (83.6 and 87.3 eV) for gold nanoparticles adsorbed onto the surfaces [36] and the Si 2p peak (102.5 eV) of the substrate. Satisfyingly, the comparison between the surface coverage estimated by AFM and XPS reveals a good agreement between the two independent sets of data as reported in figure 9(a)–(f) and summarized in table 3.

Considering that the X-ray beam has a diameter of 500 μm it allows a much larger sampling area ($2.0 \times 10^{11} \text{ nm}^2$) for the determination of the surface coverage, compared to the AFM ($2.5 \times 10^5 \text{ nm}^2$) methodology. For this reason greater confidence can be given to the relative surface coverage results from the XPS data.

3.3.1. Si/SiO₂ surface. AFM images of Si/SiO₂ substrates immersed in citrate- and acrylate-stabilized gold nanoparticles at different pHs are shown in figure 6(a) and (b). AFM and XPS analysis indicated that gold nanoparticle deposition does not take place appreciably on Si/SiO₂ substrates over the range of pH explored (figure 9a and b and table 3). The only exception is represented by acrylate-stabilized gold nanoparticles at pH 3.0 which show a disagreement between the surface coverage data collected by AFM and XPS as illustrated in figure 9(b). As mentioned previously, the XPS data were collected from a much larger sampling area compared with the AFM methodology. Thus, XPS data for surface coverages are more reliable in a quantitative sense. The correlation of the XPS data with the AFM data suggests that acrylate particles exhibit a surface coverage of $\sim 4.7\%$ at pH 3.0.

3.3.2. Nitro-terminated surface. AFM images of NPPTMS monolayers immersed in citrate- and acrylate-gold nanoparticles are reported in figure 7(a) and (b). A comparison of the surface coverage for the two types of particles estimated by AFM and XPS is reported in figure 9(c) and (d) and table 3. This data revealed that citrate-stabilized gold nanoparticles do not deposit appreciably on nitro-terminated surfaces exhibiting a maximum surface coverage of $0.77 \pm 0.40\%$ by AFM with strong correlation with the XPS data. Acrylate-stabilized gold nanoparticles tend to be immobilized on nitro-terminated surfaces at pH lower than 3.5 with a surface coverage of $3.7 \pm 4.7\%$ and $4.4 \pm 2.0\%$ at pH 3.0 and pH 3.5, respectively, which is correlated with the XPS data.

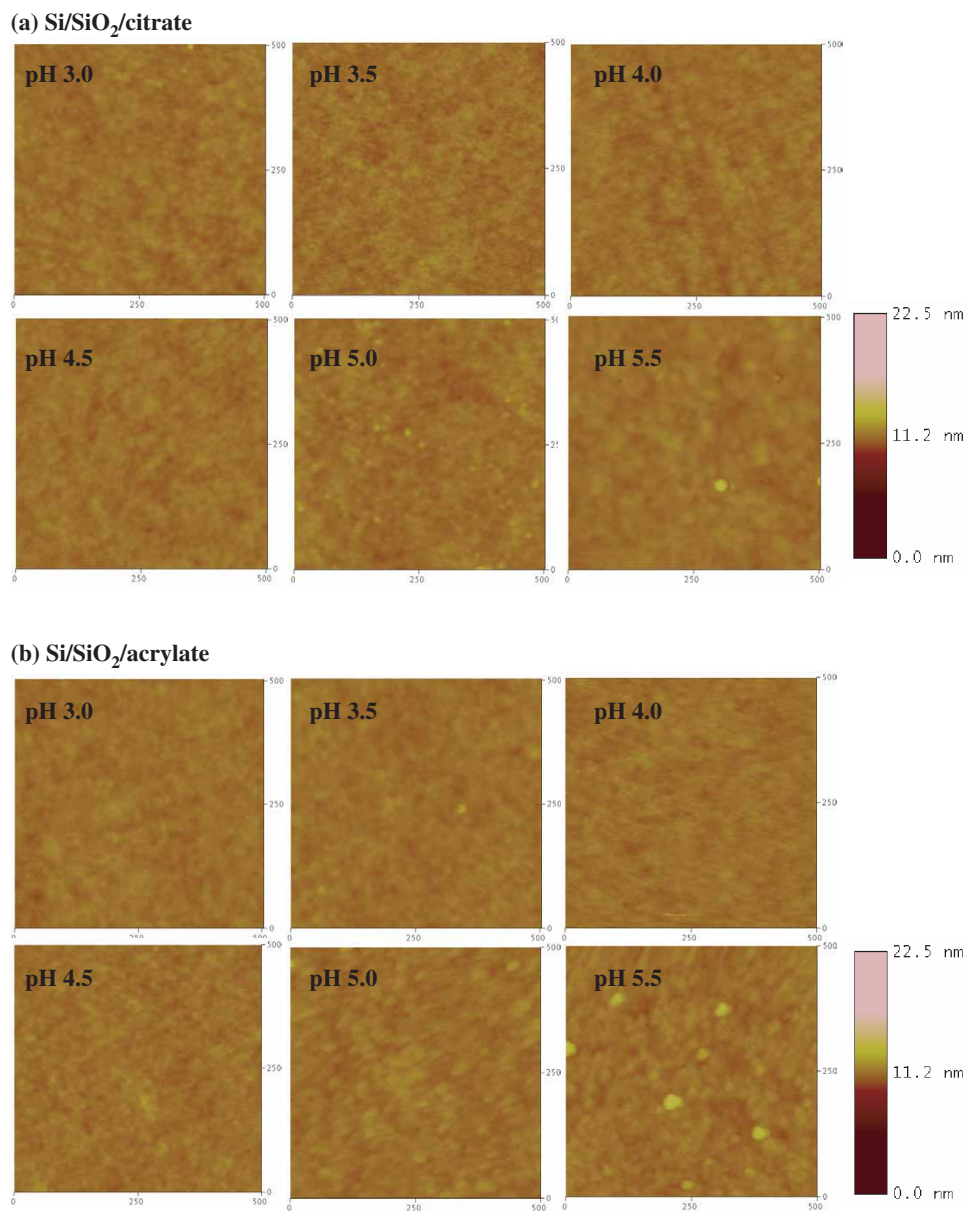


Figure 6. Tapping mode AFM images (500 nm \times 500 nm) of Si/SiO₂ surfaces immersed in (a) citrate- and (b) acrylate-stabilized gold nanoparticle solutions at different pHs.

3.3.3. Amino-terminated surface. AFM images of amino-terminated surfaces immersed in citrate- and acrylate-stabilized gold nanoparticles solutions at different pHs are shown in figure 8(a) and (b). Since the amino groups of an aliphatic amine (pK_a 10–11) are fully protonated under the range of pHs explored in this study, electrostatic

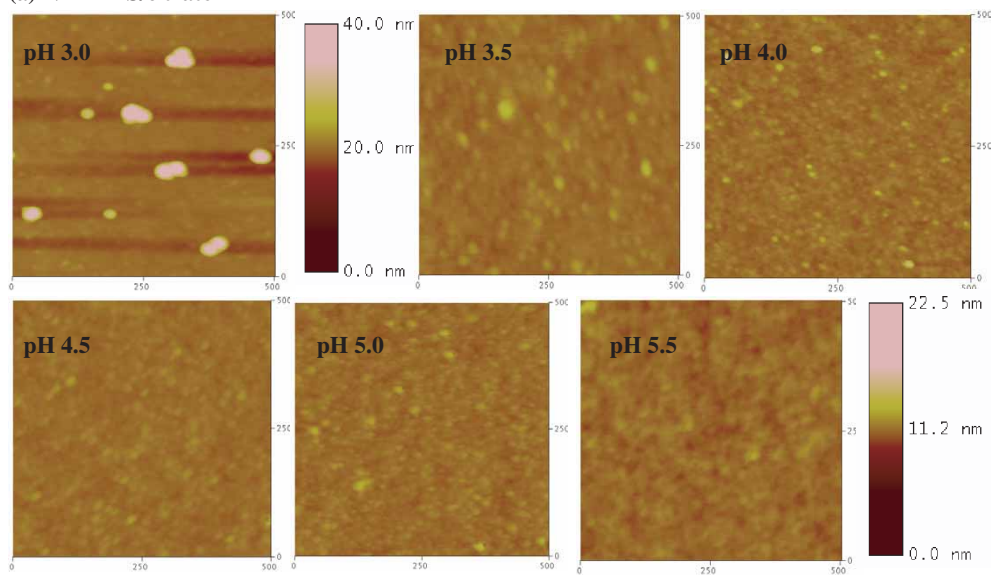
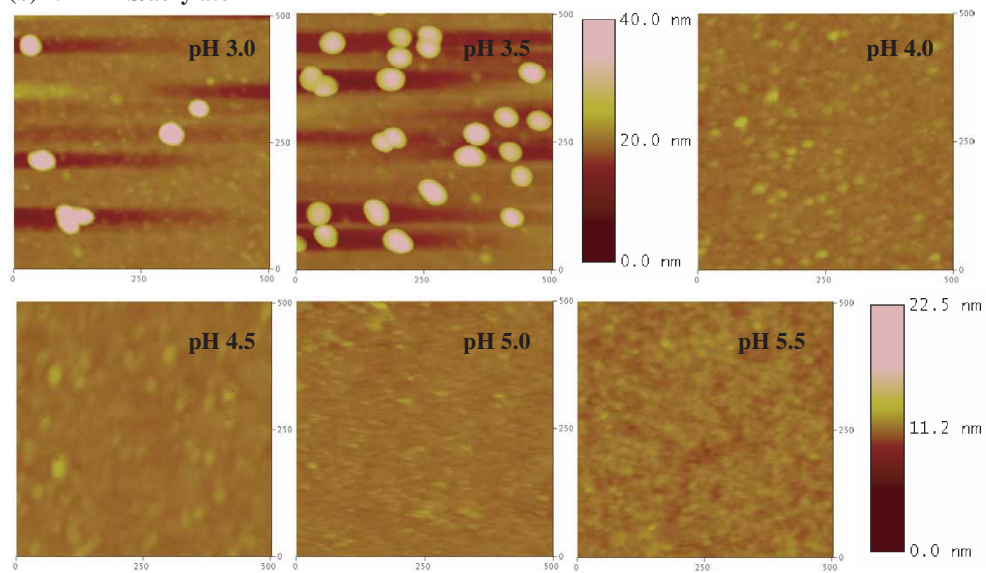
(a) NPPTMS/citrate**(b) NPPTMS/acrylate**

Figure 7. Tapping mode AFM images (500 nm × 500 nm) of NPPTMS monolayers immersed in (a) citrate- and (b) acrylate-stabilized gold nanoparticle solutions at different pHs. The z-scale bar for pH 3.0 is to the right of the image. The z-scale bar for pHs from 3.5 to 5.5 is to the right of the image of pH 5.5.

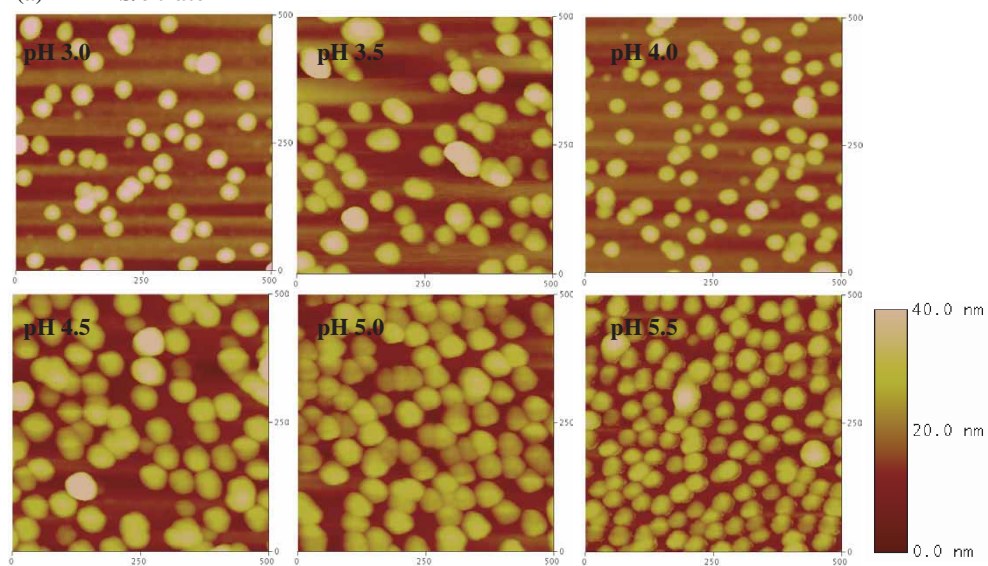
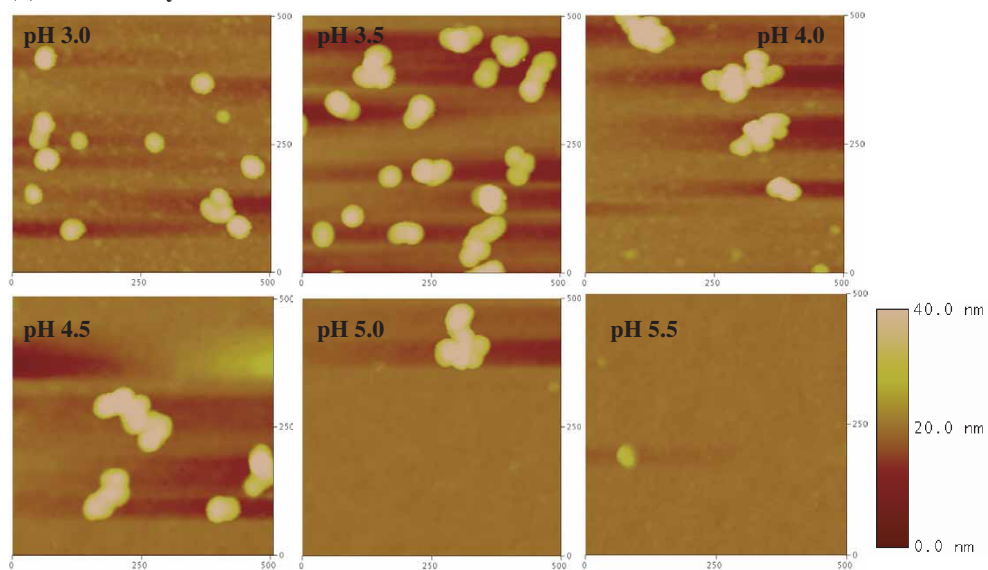
(a) APTMS/citrate**(b) APTMS/acrylate**

Figure 8. Tapping mode AFM images ($500\text{ nm} \times 500\text{ nm}$) of APTMS monolayers immersed in (a) citrate- and (b) acrylate-stabilized gold nanoparticle solutions at different pHs. The z -scale bar for pH 3.0 and pH 3.5 is to the right of the image of pH 3.5. The z -scale bar for pHs from 4.0 to 5.5 is to the right of the image of pH 5.5.

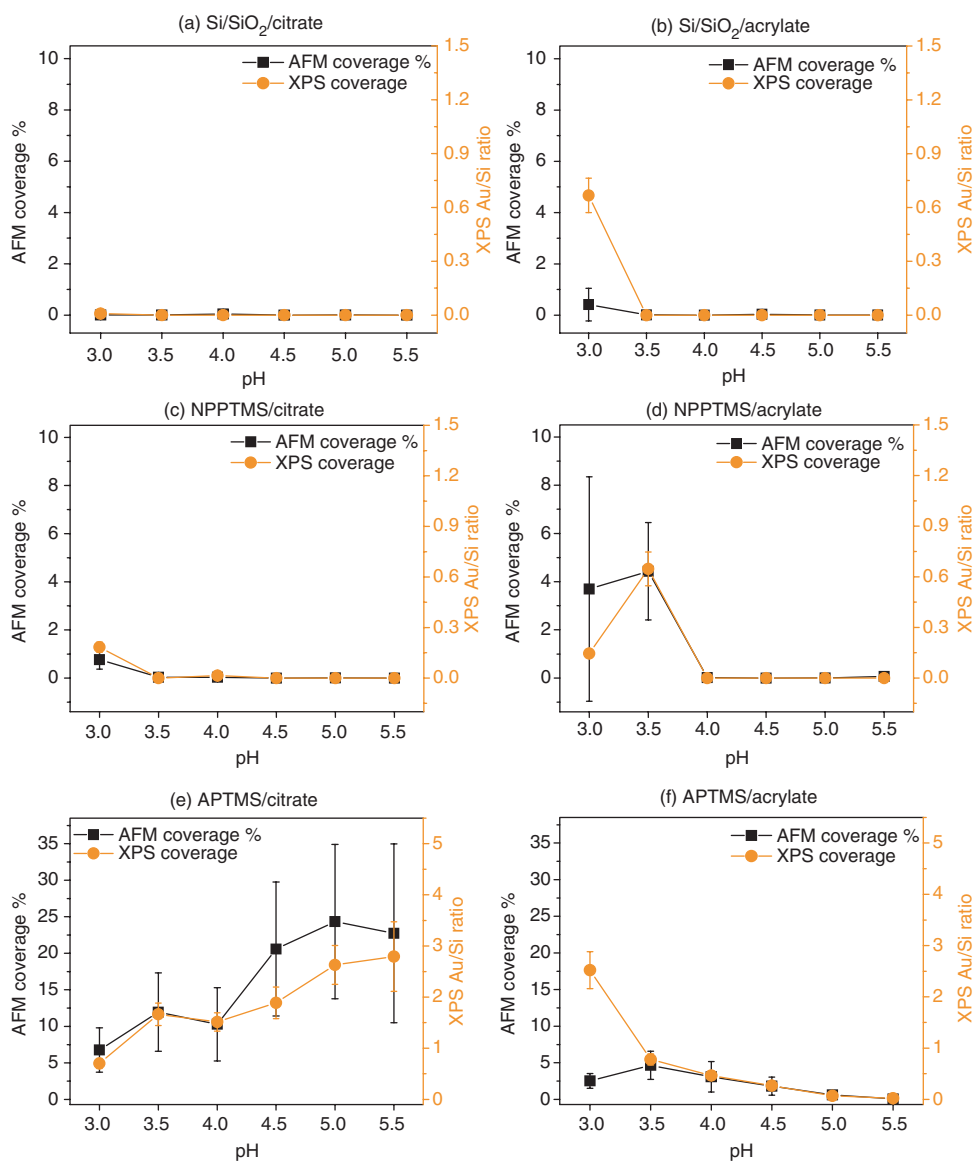


Figure 9. Surface coverage estimated by AFM and by XPS (as gold to silicon ratio) for Si/SiO₂ surfaces immersed in (a) citrate- and (b) acrylate-stabilized gold nanoparticles, NPPTMS monolayers immersed in (c) citrate- and (d) acrylate-stabilized gold nanoparticles and APTMS monolayers immersed in (e) citrate and (f) acrylate-stabilized gold nanoparticle solutions, at different pHs. The XPS coverages shown above were scaled in order to allow direct comparison with the AFM coverages. This was achieved by multiplying the XPS data by an arbitrary scaling factor and calculating the residuals between the AFM and XPS coverages at each pH. The best value for the scaling factor was then found by minimizing the standard deviation of the data set. Thus, XPS data points can be directly read across to AFM percentage coverages.

Table 3. AFM and XPS coverage of hydroxyl-, nitro- and amino-terminated surfaces immersed in citrate- and acrylate-stabilized gold nanoparticles solutions at different pHs.

	Citrate-stabilized gold nanoparticles				Acrylate-stabilized gold nanoparticles			
	SiO ₂ (OH)	NO ₂	NH ₂		SiO ₂ (OH)	NO ₂	NH ₂	
pH 3.0	AFM	0.0041 ± 0.0084	0.77 ± 0.40	6.8 ± 3.0	0.41 ± 0.63	3.7 ± 4.7	2.5 ± 1.0	
	XPS	0.0082 ± 0.0051	0.184 ± 0.030	0.702 ± 0.098	0.667 ± 0.096	0.145 ± 0.016	2.52 ± 0.36	
pH 3.5	AFM	0.0041 ± 0.0073	0.0319 ± 0.044	12.0 ± 5.4	0.007 ± 0.016	4.4 ± 2.0	4.7 ± 1.9	
	XPS	0	0	1.66 ± 0.22	0	0.65 ± 0.10	0.78 ± 0.11	
pH 4.0	AFM	0.040 ± 0.076	0.032 ± 0.051	10.3 ± 5.0	0	0.017 ± 0.022	3.1 ± 2.1	
	XPS	0	0.0139 ± 0.0092	1.51 ± 0.18	0	0	0.464 ± 0.078	
pH 4.5	AFM	0	0.0010 ± 0.0029	20.6 ± 9.2	0.036 ± 0.070	0.0021 ± 0.0042	1.8 ± 1.2	
	XPS	0	0	1.89 ± 0.31	0	0	0.268 ± 0.036	
pH 5.0	AFM	0.0012 ± 0.0031	0.0055 ± 0.0097	24 ± 11	0.0028 ± 0.0069	0.0042 ± 0.0094	0.62 ± 0.47	
	XPS	0	0	2.63 ± 0.38	0	0	0.068 ± 0.011	
pH 5.5	AFM	0	0.0014 ± 0.0034	23 ± 12	0.0042 ± 0.0084	0.07 ± 0.14	0.07 ± 0.12	
	XPS	0	0	2.79 ± 0.68	0	0	0.023 ± 0.015	

interactions between the negatively charged nanoparticles and the positively charged surface NH₃⁺ groups are expected to dominate the colloid deposition onto this substrates.

Citrate stabilized gold nanoparticles show a strong dependence on adsorption to APTMS surfaces as a function of pH by both AFM and XPS. Increasing pH results in increasing surface adsorption up to ~25%. In contrast, acrylate stabilized gold nanoparticles revealed the opposite trend as the pH increases. Between pH 3.0 and 5.5 the surface coverage drops from ~5.0% to zero (figure 9f).

According to zeta potential measurements, citrate- and acrylate-stabilized gold nanoparticles did not present a substantial difference in the surface charge that could rationalize their different absorption behaviour as function of pH (figure 3). Thus, the absorption phenomenon is not being dictated by electrostatic interactions. However, a closer look at the AFM images reveals that acrylate-stabilized gold nanoparticles appear to aggregate on the amino-terminated surfaces (figure 8b) to a greater extent than citrate-stabilized gold nanoparticles (figure 8a). Thus, it is clear that the adsorption process is more complex than just considering simple electrostatic interactions between the particles and the surface. For example, the acrylate-stabilized gold nanoparticles undoubtedly present a more hydrophobic surface virtue of the alkene moiety, leading possibly to the observed aggregation behaviour.

It is noteworthy to consider that the citrate-stabilized gold nanoparticle surface adsorption behaviour to APTMS SAMs is opposite to the one previously reported from Zhu *et al.* for the deposition of the same particles on p-aminothiophenol monolayers on gold [10]. The main difference between the two systems is the pK_a of the amino-terminated surfaces. p-Aminothiophenol has a solution pK_a of 5.3 and the progressive protonation of the surface from pH 5.5 to pH 3.0 dominates the electrostatic immobilization of the colloid. In the experiments reported here, an aliphatic amine has been used (solution pK_a of 10–11) which is expected to be protonated to a much greater extent than an aromatic amine, under the range of pHs explored (5.5 to 3.0). Whereas, the citrate-stabilized gold nanoparticles become more negatively charged as the pH increases, enhancing the interaction with the positively charged amino-surface. It is interesting to note that the opposite behaviour is observed here for acrylate-stabilized gold nanoparticles (figure 9f). This behaviour is in contrast with an interpretation based on simple electrostatic interactions governing the immobilization of acrylate-stabilized gold nanoparticles. As noted previously this may be due to the surface mediated aggregation behaviour of the acrylate-stabilized gold nanoparticles.

4. Conclusions

In this study, the pH-dependent immobilization of citrate- and acrylate-stabilized gold nanoparticles from solution onto hydroxyl-, nitro- and amine-terminated surfaces were investigated. It has been shown that bare Si/SiO₂ surfaces exhibit very little or no nanoparticle surface coverage over the range of pH explored. Moreover no strong interactions were found between citrate-stabilized gold nanoparticles and the nitro-terminated monolayers. Acrylate-stabilized gold nanoparticles were found to be immobilized on nitro-terminated surfaces only at a pH lower than 3.5.

The amino-terminated monolayers interacted strongly with citrate-stabilized gold nanoparticles exhibiting an increase in surface coverage with increasing pH. On amino-terminated surfaces, the absorption of acrylate-stabilized gold nanoparticles was found to be less efficient compared with citrate-stabilized gold nanoparticles. Acrylate-stabilized gold nanoparticle immobilization was also accompanied by particle aggregation on both nitro- and amino-terminated surfaces, unlike the citrate stabilized gold nanoparticles. This behaviour may be accounted for by the facts that (i) the acrylate stabilizer is not as charged as the citrate stabilizer, and (ii) the alkene moiety results in the surface of the acrylate-stabilized gold nanoparticles being considerably more hydrophobic. In addition, the surface coverage showed a reverse pH dependence of citrate-stabilized gold nanoparticles on the amino terminated surface, relative to the acrylate-stabilized gold nanoparticles. Therefore, when considering such charge stabilized nanoparticles and their absorption onto surfaces one has to take into account more than just simple electrostatic arguments.

The present work represents a fundamental study on the deposition of colloidal particles from solution onto different substrates of well-defined surface chemistry under a range of conditions. This research contributes to furthering our knowledge on the surface adsorption behaviour of colloidal particles on to various surfaces. Such studies will allow a predictive power to be developed and used in the design of three-dimensional nano-architectures.

Acknowledgements

This work was financially sponsored by EU grants Micro-Nano HPRN-CT-2000-00028 and Nano3D STRP 014006, and BAE SYSTEMS.

References

- [1] P.M. Mendes, Y. Chen, R.E. Palmer, K. Nikitin, D. Fitzmaurice, J.A. Preece. Nanostructures from nanoparticles. *J. Phys.: Condens. Matter*, **15**, S3047 (2003).
- [2] M. Veiseh, M.H. Zareie, M. Zhang. Highly selective protein patterning on gold–silicon substrates for biosensor applications. *Langmuir*, **18**, 6671 (2002).
- [3] P. Vettiger, G. Binning. Inventing a nanotechnology device for mass production and consumer use is trickier than it sounds. *Scient. Amer.*, **1**, 35 (2003).
- [4] D.L. Feldheim, C.D. Keating. Self-assembly of single electron transistors and related devices. *Chem. Soc. Rev.*, **27**, 1 (1998).
- [5] P. Ball. Chemistry meets computing. *Nature*, **406**, 118 (2000).
- [6] P.M. Mendes, J.A. Preece. Precision chemical engineering: integrating nanolithography and nanoassembly. *Curr. Opin. Colloid Interface Sci.*, **9**, 236, and references herein (2004).
- [7] P.M. Mendes, M. Belloni, M. Ashworth, C. Hardy, K. Nikitin, D. Fitzmaurice, K. Critchley, S.D. Evans, J.A. Preece. A novel example of X-ray radiation induced chemical reduction of an aromatic nitro containing thin film on SiO₂ to an aromatic amine film. *Chem. Phys. Chem.*, **4**, 884 (2003).
- [8] P.M. Mendes, S. Jacke, K. Critchley, J. Plaza, Y. Chen, K. Nikitin, R.E. Palmer, J.A. Preece, S.D. Evans, D. Fitzmaurice. Gold nanoparticle patterning of silicon wafers using chemical e-beam lithography. *Langmuir*, **20**, 3766 (2004).
- [9] H. Fan, G.P. Lopez. Adsorption of surface-modified colloidal gold particles onto self-assembled monolayers: a model system for the study of interactions of colloidal particles and organic surfaces. *Langmuir*, **13**, 119 (1997).
- [10] T. Zhu, X. Fu, T. Mu, J. Wang, Z. Liu. pH-Dependent adsorption of gold nanoparticles on p-aminothiophenol-modified gold substrates. *Langmuir*, **15**, 5197 (1999).

- [11] R.M. Bright, M.D. Musick, M.J. Natan. Preparation and characterization of Ag colloid monolayers. *Langmuir*, **14**, 5695 (1998).
- [12] K.C. Grabar, P.C. Smith, M.D. Musick, J.A. Davis, D.G. Walter, M.A. Jackson, A.P. Guthrie, M.J. Natan. Kinetic control of interparticle spacing in Au colloid-based surfaces: rational nanometer-scale architecture. *J. Am. Chem. Soc.*, **118**, 1148 (1996).
- [13] G. Frens. Controlled nucleation for the regulation of the particles size in monodisperse gold suspensions. *Nature Phys. Sci.*, **241**, 20 (1973).
- [14] I. Hussain, M. Brust, A.J. Papworth, A.I. Cooper. Preparation of acrylate-stabilized gold and silver hydrosols and gold-polymer composite films. *Langmuir*, **19**, 831 (2003).
- [15] A. Ulman, *An Introduction to Ultrathin Organic Films*, Academic Press, London (1991).
- [16] N. Tillman, A. Ulman, J.F. Elman. A novel self-assembling monolayer film containing a sulfone-substituted aromatic group. *Langmuir*, **6**, 1512 (1990).
- [17] F. Pintchovski, J.B. Price, P.J. Tobin, J. Peavey, K. Kobold. *J. Electrochem. Soc.*, **126**, 1428 (1979).
- [18] A.G. Richter. An examination of the process of self-assembly using X-rays. PhD thesis, Northwestern University Evanston, Illinois (2000).
- [19] A.N. Shipway, E. Katz, I. Willner. An examination of the process of self-assembly using X-rays. *Chem. Phys. Chem.*, **1**, 18 (2000).
- [20] M.-C. Daniel, D. Astruc. Gold nanoparticles: assembly, supramolecular chemistry, quantum-size-related properties, and applications toward biology, catalysis, and nanotechnology. *Chem. Rev.*, **104**, 293 (2004).
- [21] P. Mulvaney. Surface plasmon spectroscopy of nanosized metal particles. *Langmuir*, **12**, 788 (1996).
- [22] K.G. Thomas, P.V. Kamat. Making gold nanoparticles glow: enhanced emission from a surface-bound fluoroprobe. *J. Am. Chem. Soc.*, **122**, 2655 (2000).
- [23] D.A. Weitz, M.Y. Lin. Colloidal aggregation revisited: new insights based on fractal structure and surface-enhanced Raman scattering. *Surface Sci.*, **158**, 147 (1985).
- [24] D.H. Everett. *Basic Principles of Colloid Science*, The Royal Society of Chemistry, London (1988).
- [25] M.K. Chow, C.F. Zukoski. Gold sol formation mechanisms: role of colloidal stability. *J. Colloid Interface Sci.*, **165**, 97 (1994).
- [26] Q. Li, Z. Liu. Site-selective assemblies of gold nanoparticles on an AFM tip-defined silicon template. *Langmuir*, **19**, 166 (2003).
- [27] N.E. Cant, K. Critchley, H.-L. Zhang, S.D. Evans. Surface functionalisation for the self-assembly of nanoparticle/polymer multilayer films. *Thin Solid Films*, **426**, 31 (2003).
- [28] P. Silberzan, L. Leger, D. Ausserre, J.J. Benattar. Silanation of silica surfaces. A new method of constructing pure or mixed monolayers. *Langmuir*, **7**, 1647 (1991).
- [29] D.L. Angst, G.W. Simmons. Moisture absorption characteristics of organosiloxane self-assembled monolayers. *Langmuir*, **7**, 2236 (1991).
- [30] A. Ulman. Formation and structure of self-assembled monolayers. *Chem. Rev.*, **96**, 1533 (1996).
- [31] A.B. Sieval, R. Linke, G. Heij, G. Meijer, H. Zuilhof, E.J.R. Sudholter. Amino-terminated organic monolayers on hydrogen-terminated silicon surfaces. *Langmuir*, **17**, 7554 (2001).
- [32] R. Banga, J. Yarwood, A.M. Morgan, B. Evans, J. Kells. FTIR and AFM studies of the kinetics and self-assembly of alkyltrichlorosilanes and (perfluoroalkyl)trichlorosilanes onto glass and silicon. *Langmuir*, **11**, 4393 (1995).
- [33] P.E. Laibinis, R.L. Graham, H.A. Biebuyck, G.M. Whitesides. X-Ray damage to CF₃CO₂-terminated organic monolayers on Si/Au: principal effects of electrons. *Science*, **254**, 981 (1991).
- [34] J. Wang, T. Zhu, J. Song, Z. Liu. Gold nanoparticulate film bound to silicon surface with self-assembled monolayers. *Thin Solid Films*, **327–329**, 591 (1998).
- [35] D. Keller. Reconstruction of STM and AFM images distorted by finite-size tips. *Surf. Sci.*, **253**, 353 (1991).
- [36] Y. Joseph, I. Besnard, M. Rosenberger, B. Guse, H.-G. Nothofer, J.M. Wessels, U. Wild, A. Knop-Gericke, D. Du, R. Schlögl, A. Yasuda, T. Vossmeier. Self-assembled gold nanoparticle/alkanedithiol films: preparation, electron microscopy, XPS-analysis, charge transport, and vapor-sensing properties. *J. Phys. Chem. B*, **107**, 7406 (2003).